Geophys. J. Int. (1997) **128**, 204–216

Dynamic nucleation process of shallow earthquake faulting in a fault zone

Nobuki Kame and Teruo Yamashita

Earthquake Research Institute, University of Tokyo, 1-1-1 *Yayoi, Bunkyo-Ku, Tokyo* 113, *Japan*

Accepted 1996 September 16. Received 1996 September 10; in original form 1995 November 20

SUMMARY

Two distinct phases are commonly observed at the initial part of seismograms of large shallow earthquakes: low-frequency and low-amplitude waves following the onset of a P wave (P_1) are interrupted by the arrival of the second impulsive phase P_2 enriched with high-frequency components. This observation suggests that a large shallow earthquake involves two qualitatively different stages of rupture at its nucleation.

We propose a theoretical model that can naturally explain the above nucleation behaviour. The model is 2-D and the deformation is assumed to be anti-plane. A key element in our model is the assumption of a zone in which numbers of pre-existing cracks are densely distributed; this cracked zone is a model for the fault zone. Dynamic crack growth nucleated in such a zone is intensely affected by the crack interactions, which exert two conflicting effects: one tends to accelerate the crack growth, and the other tends to decelerate it. The accelerating and decelerating effects are generally ascribable to coplanar and non-coplanar crack interactions, respectively. We rigorously treat the multiple interactions among the cracks, using the boundary integral equation method (BIEM), and assume the critical stress fracture criterion for the analysis of spontaneous crack propagation.

Our analysis shows that a dynamic rupture nucleated in the cracked zone begins to grow slowly due to the relative predominance of non-coplanar interactions. This process radiates the P_1 phase. If the crack continues to grow, coalescence with adjacent coplanar cracks occurs after a short time. Then, coplanar interactions suddenly begin to prevail and crack growth is accelerated; the P_2 phase is emitted in this process. It is interpreted that the two distinct phases appear in the process of the transition from non-coplanar to coplanar interaction predominance.

Key words: cracks, fault models, fractures, rupture propagation.

INTRODUCTION

It has recently become possible to detect a phase in seismograms associated with dynamic nucleation of large shallow earthquakes, because of the installation of seismographs with sufficient dynamic range and bandwidth (Umeda 1990, 1992; Abercrombie & Mori 1994; Ellsworth & Beroza 1995). We can therefore derive from such observations some information about the dynamic nucleation process of earthquake rupture. Here, the term dynamic nucleation stands for the initial growth stage of earthquake rupture that radiates seismic waves. The initial part of vertical velocity seismograms of the 1984 Western Nagano earthquake is shown in Fig. 1(a) as an example. We can see the low-frequency and low-amplitude waves following the symbol P_1, and the high-frequency and high-amplitude waves following the symbol P_2; these two phases are commonly identified for this earthquake on seismograms recorded at various stations with different distances and azimuths. It was confirmed that these two phases have their origins at the earthquake source (Umeda 1990). Another example is shown in Fig. 1(b) for the 1990 Philippine earthquake. These two distinct phases have been commonly found for many large shallow earthquakes by Umeda (1990, 1992) who inferred, on the basis of seismological observations of these phases, that a large shallow earthquake involves two qualitatively different stages of rupture at its nucleation. Umeda (1990, 1992) interpreted the P_1 phase as corresponding to a relatively slow preliminary rupture process. The phase beginning with P_2 was termed the 'bright spot phase' by Umeda *et al.* (1996), since it seems to be closely related to the formation of the earthquake bright spot. The earthquake bright spot is defined as a small region near the epicentre where strong seismic waves are radiated (Umeda 1981, 1990, 1992; Umeda *et al.* 1987). It has been inferred from the observation of boulders thrown up by

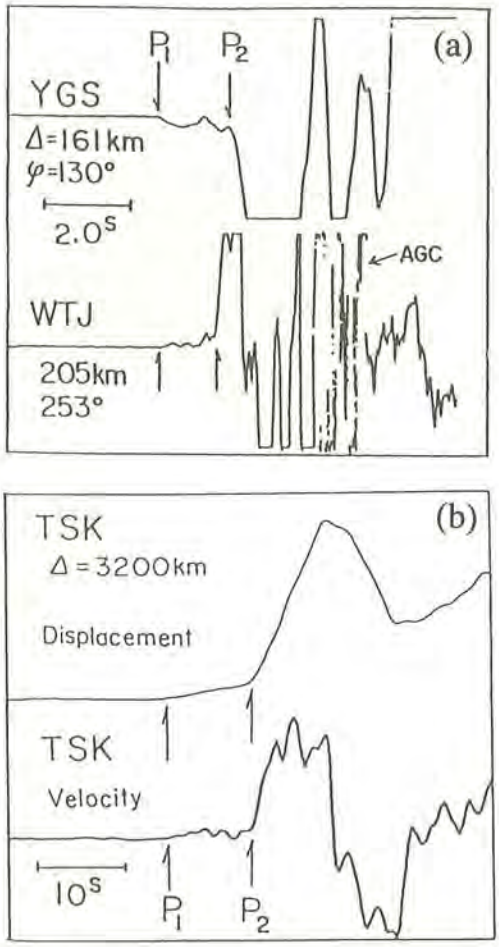

Figure 1. (a) Vertical velocity seismograms near the arrival time of *P* waves radiated from the main shock ($M = 6.8$) of the 1984 Western Nagano earthquake (after Umeda 1990). AGC denotes auto-gain control. The epicentral distance and azimuth of each station are shown by Δ and ϕ, respectively. (b) Vertical seismograms of the 1990 Philippine earthquake ($M = 7.8$). The original seismograms are from Abe (1990).

shaking (Umeda 1992) that the highest ground acceleration caused by the bright spot phase occasionally exceeds the Earth's gravity.

It is obvious that the above two phases cannot be explained by theoretical fault models in which source parameters are spatio-temporally invariable. Shibazaki & Matsu'ura (1994) tried to simulate the slow dynamic nucleation process by assuming an isolated fault and applying a spatially heterogeneous constitutive law of a slip-weakening type to it. However, modelling with an isolated fault reveals only an average overall structure of earthquake rupture. It is now increasingly clear from both theoretical modelling and seismological observation that the consideration of a fault as an isolated system is inappropriate (Scholz 1990; Harris, Archuleta & Day 1991; Harris & Day 1993; Yamashita & Umeda 1994; Yamashita 1995; Umeda *et al.* 1996). In fact, it is observed that a major crustal fault is not a single fault but forms a fault zone (e.g. Tchalenko 1970; Tchalenko & Berberian 1975). A fault zone is generally considered as a region of increased crack density compared to the nearby crust (e.g. Rice 1992; Leary, Li & Aki 1987). Leary *et al.* (1987) analysed borehole seismograms recorded in the vicinity of an active fault in California, and showed that cracks are aligned predominantly parallel to the fault plane. In addition it is believed that the pre-existing cracks grew quasi-statically into larger ones, due to stress corrosion cracking, at the epicentral area of the eventual earthquake immediately before its occurrence (Yamashita & Knopoff 1992). Hence, dynamic crack growth nucleated in a fault zone should be intensely affected by the crack interactions. In this paper, we construct a fault model as an interactive system and study how crack interactions affect the initial stage of dynamic fault growth.

The crack interactions mainly depend on the relative geometry of the cracks. The fundamental mechanism of the dynamic crack interactions can be inferred to some degree from the static analysis of two interactive cracks. Static stress fields around two neighbouring cracks are illustrated in Fig. 2 for three typical crack configurations. In all cases, the shear stress is commonly enhanced outside the crack near the tips, while it is released down to the residual stress level near the crack traces. When two cracks are coplanar and close to each other, as illustrated in Fig. 2(a), a much higher stress is observed in the narrow zone between the inner tips than in the absence of the interaction. This is because each inner crack tip is located in the zone of increased stress formed by the other crack. Therefore, dynamic growth of the cracks is inclined to be accelerated, and catastrophic rupture is expected to take place at the inner crack tips. On the other hand, when two nearby cracks are non-coplanar and overlapping, as illustrated in Fig. 2(b), the stress near the inner tips is much lower than in the absence of the interaction: each inner tip is located in the zone of decreased stress formed by the other crack. The zone of decreased stress near a crack trace is referred to as the 'stress shadow' in this paper, after the terminology of Yamashita & Umeda (1994). Therefore, the occcurrence of catastrophic rupture at the inner tips tends to be suppressed in the configuration, as illustrated in Fig. 2(b). If one of the two cracks lies entirely in the stress shadow of the other, the growth of the former is almost entirely suppressed and the interaction is almost unilateral from the latter to the former (see Fig. 2c).

Our analysis will show that the crack interactions considerably affect the dynamic nucleation of rupture in a fault zone. The two distinct phases observed on seismograms of large shallow earthquakes will naturally be understood as a manifestation of the crack interactions in a fault zone.

A FAULT ZONE MODEL

2-D, anti-plane deformation is considered below. The medium is assumed to be elastic, homogeneous, isotropic and infinite. As stated in the preceding section, the active part of a fault forms a fault zone, which is characterized by densely distributed cracks that predominantly align parallel to the fault strike. Accordingly, we construct a fault zone model as a zone in which parallel pre-existing anti-plane Griffith cracks are densely distributed. We refer to the distribution zone of the cracks as the 'cracked zone'. An example of the assumed cracked zone is illustrated in Fig. 3(a). We take a Cartesian coordinate system (x, y, z) in the medium with the rigidity μ. We take the centre plane of the cracked zone as $y = 0$, and the direction of relative slip and crack extension are taken to be parallel to the z- and x-axes, respectively. The cracked zone contains N cracks, which are numbered $1, 2, \ldots, N$. The pth

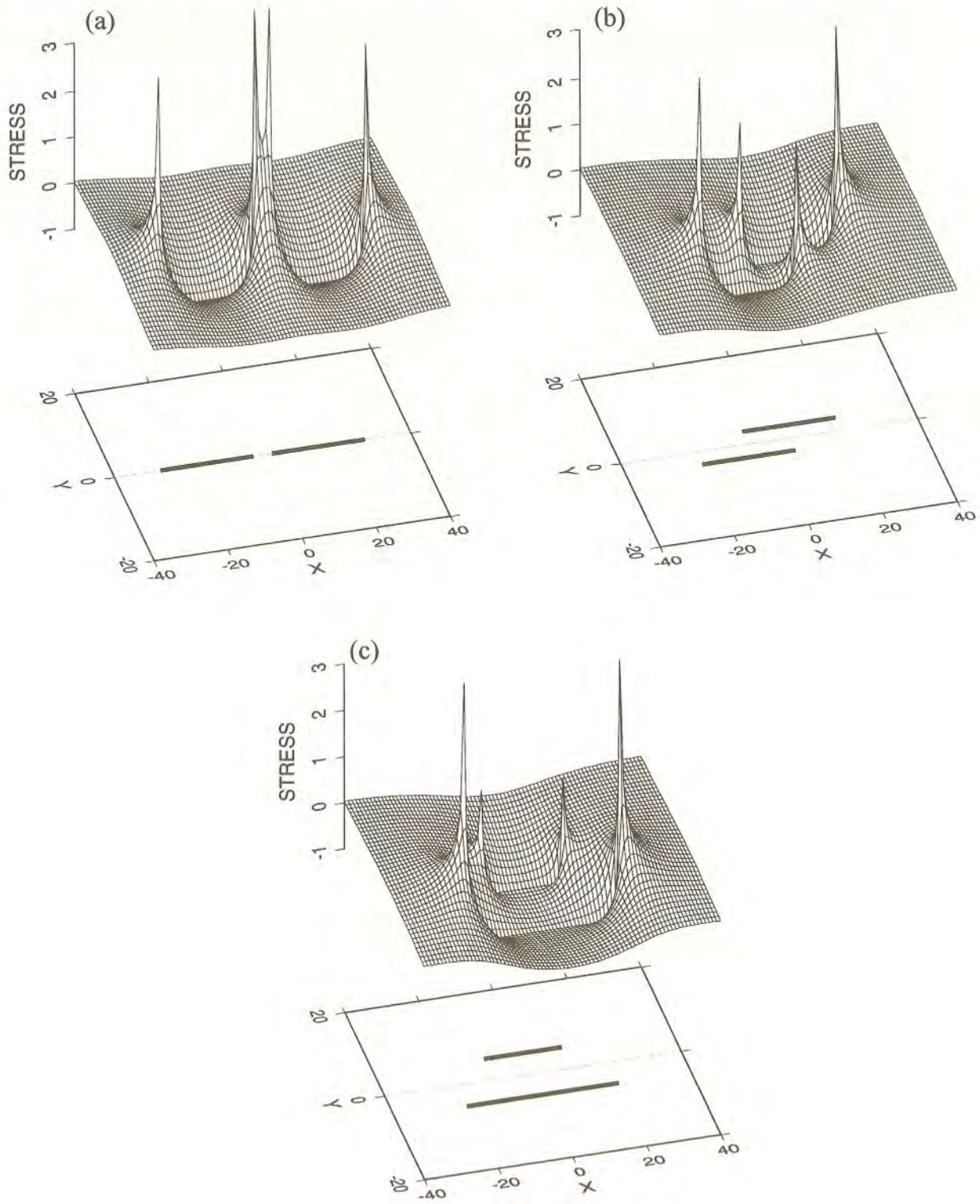

Figure 2. Static stress fields caused by two interactive anti-plane cracks of three types of geometry: non-dimensional physical quantities are used and a unit stress drop is assumed to occur on each crack. (a) Coplanar cracks. (b) Half-overlapped non-coplanar cracks. (c) Non-coplanar cracks: the smaller crack is thoroughly overlaid by the other.

crack has its centre at (x_p, y_p). All the pre-existing cracks are assumed to have the same length, and the same stress drop is assumed to occur over this length. We set the same spacing of the crack centres in the x-direction on each crack array, and the same crack array spacing in the y-direction. However, the relative location of the cracks in the x-direction on different arrays is assumed to obey a homogeneous statistical distribution. The spacing in the y-direction is set to be shorter than in the x-direction. Note that the effect of non-coplanar interactions is relatively dominant in this crack distribution. It will

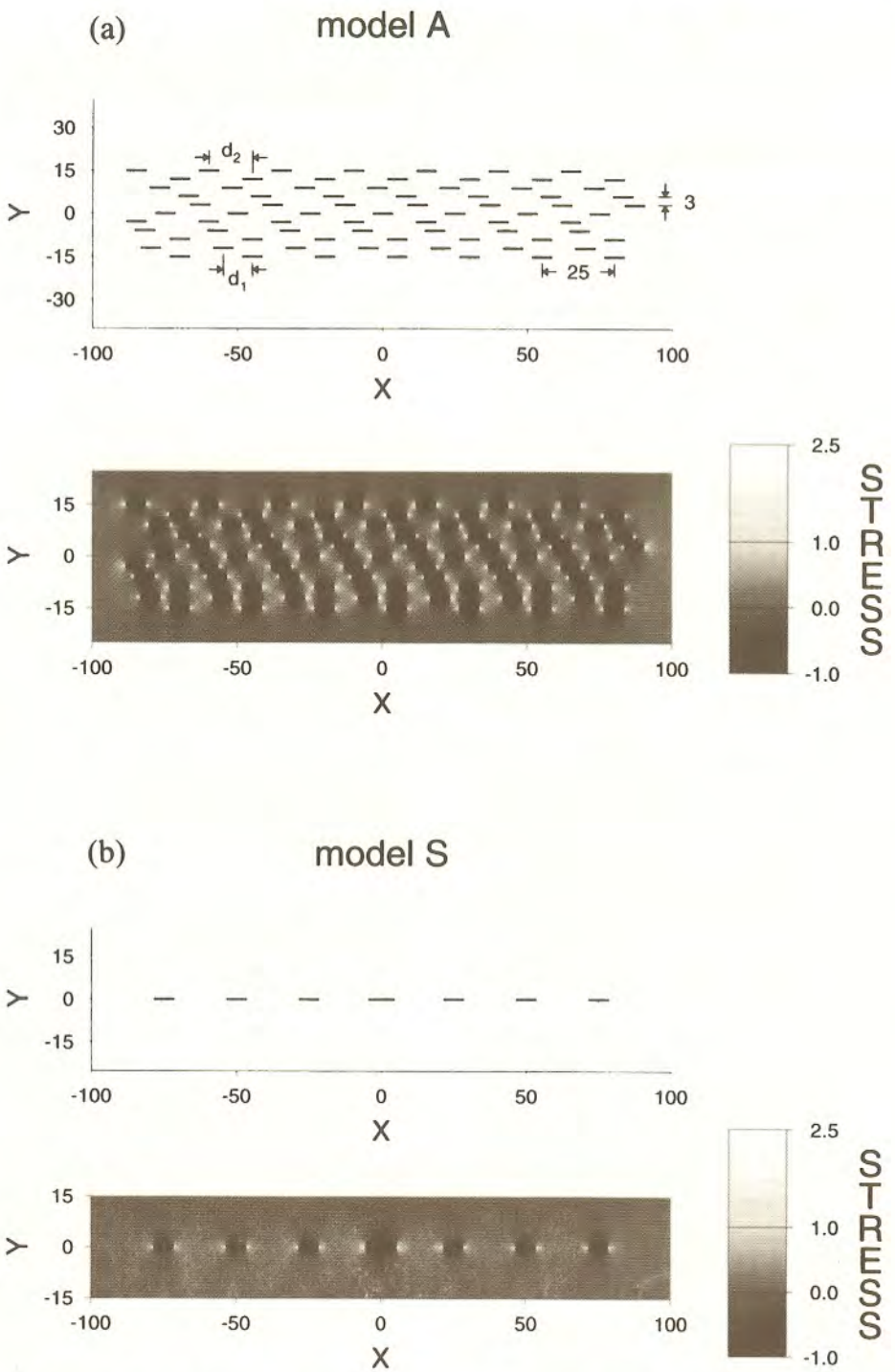

Figure 3. An example of the assumed cracked zone, model A. Each line segment denotes a pre-existing crack, and the corresponding static stress field is illustrated in the lower figure. The cracks are distributed in the range $-15 \leq Y \leq 15$, so that the non-dimensional cracked zone width is 30. All the cracks are assumed to have the same length, 7. We fix the spacing of the crack centres at 25 on each crack array, and the crack array spacing at 3. However, the relative location of cracks in the X-direction on different arrays, such as d_1 or d_2, is assumed to obey a homogeneous random distribution. (b) A reference model S, which consists only of a coplanar crack array. The static stress field due to this crack configuration is shown in the lower figure. A slightly large crack length of 9 is assumed for the central crack in order to initiate the rupture there.

be shown later that such a distribution is appropriate for a model of a fault zone just before the occurrence of a large shallow earthquake. Once a rupture is nucleated, it grows in the form of dynamic coalescence with neighbouring coplanar cracks. The slip on each crack is assumed to be unlocked; in other words, slip is assumed to occur freely on each crack. A locked crack that does not slip is perfectly transparent for a seismic wave and therefore does not interact dynamically at

all. We accordingly take only unlocked cracks in the cracked zone, since locked cracks do not contribute to dynamic crack interactions.

MATHEMATICAL METHOD OF ANALYSIS

The following mathematical procedure is used for the calculation of elastic waves radiated by the dynamic growth of the pre-existing interactive cracks. The calculation is carried out with normalized physical quantities (see Appendix A).

The reference state is taken to be a static uniform stress state without cracks. Only the change from this state is considered in the following analysis. At the initial state, we assume the existence of N cracks; a unit non-dimensional stress drop is assumed to occur on each crack and a static equilibrium state is assumed to be attained. These equilibrium cracks are regarded as pre-existing cracks. We carry out the calculation for their pre-slips in advance so that the static equilibrium state has been reached at time $T=0$, just before the calculation of dynamic crack growth. The method of calculation for the pre-slip is summarized in Appendix B. An example of the static stress field in the cracked zone is shown in Fig. 3(a). We can see the stress field in Fig. 3(a) due to both the coplanar and non-coplanar crack interactions. When there is only an array of coplanar cracks, the corresponding stress field is much simpler (see Fig. 3b).

The mixed boundary value problem is solved in the time domain in this paper. We rigorously treat the dynamic multiple interactions among N cracks, using the boundary integral equation method (BIEM) originally developed by Cochard & Madariaga (1994) for the analysis of an isolated crack and later extended by Yamashita & Fukuyama (1996) to incorporate the case of multiply interactive cracks. The boundary integral equation method used therein is reviewed in Appendix A.

We assume the critical stress fracture criterion for the analysis of spontaneous crack propagation as in Yamashita & Umeda (1994); that is, a crack is assumed to begin dynamic extension if the stress at the crack tip exceeds an assumed critical threshold. The critical threshold is assumed to be constant everywhere but on the plane $Y=0$ so as to enable the initiation of dynamic crack propagation on this plane. We first calculate the stresses at all the tips of the pre-existing cracks on the plane $Y=0$ and find the maximum stress value S_{main} among them. We take M_{main} slightly lower than S_{main}, as the critical threshold only on the plane $Y=0$. Except for on the plane $Y=0$, the spatially constant critical threshold M_{sub} is assumed for the whole cracked zone; M_{sub} is set to be slightly larger than S_{sub}, which is the maximum stress value at all the crack tips except on the plane $Y=0$. Applying these thresholds, M_{main} and M_{sub}, we begin the calculation of dynamic crack growth. Note that the threshold M_{main} and M_{sub} usually differ with the distribution of the cracks even if the same crack length and stress drop are assumed. This is due to the dependence of crack interactions on the crack configuration. The difference between M_{main} and M_{sub} is, however, at most 5 per cent among a variety of the assumed crack distributions. It is negligible compared with the 250–600 per cent heterogeneity on a fault plane asssumed by Das & Aki (1977) and has little influence on rupture process. We can accordingly consider the critical threshold distribution to be nearly homogeneous. Assumption of a spatially homogeneous strength distribution makes it possible for us to investigate the effect of crack interactions on irregular behaviour of dynamic nucleation, since the variable parameter is, from a practical viewpoint, only stress perturbation due to crack interactions.

DYNAMIC NUCLEATION OF RUPTURE IN THE CRACKED ZONE

We investigate how the cracks grow under the effect of crack interactions. Numerical calculations are carried out for a variety of models for pre-existing crack distributions: dynamic growth is initiated at the crack whose centre is located at $X=0$, $Y=0$ at time $T=0$ after setting up the pre-existing cracks.

We show the crack growth process for three typical examples of the distribution of the pre-existing cracks, models A, B and C. Snapshots of dynamic rupture growth are illustrated for models A, B and C at time $T=10, 20, \ldots, 80$ in Figs 4(a), (b) and (c), respectively. Each line segment represents the crack, and the thickest solid line indicates cracks that have experienced propagation. Cracks that have not propagated are classified into three types in terms of the dynamic slip caused by interactions. We assume here $I_s=\int_{\Gamma_{j_p}}\int_0^t \Delta\dot{u}_{j_p}\,d\tau\,d\xi / \int_{\Gamma_{j_p}} \Delta u_{j_p}^{\text{static}}\,d\xi$ as a measure of the amount of dynamic slip relative to the static slip just before the initiation of dynamic rupture. We arbitrarily assume $I_s>0$ and $I_s<-0.1$ to define the positively and negatively interacted cracks, which are shown by solid and grey lines of the same thickness, respectively. The others are defined as non-interacted cracks and are represented by the thinnest solid lines. The propagating crack on $Y=0$ nucleated at $X=0$ is termed the main crack and the other cracks are denoted as coplanar and non-coplanar subsidiary cracks. Here the terms 'coplanar' and 'non-coplanar' are used in terms of the main crack. Besides dynamic coalescence of the main crack with coplanar subsidiary cracks (in model A), we can see some characteristic events in the cracked zone: the main crack excites dynamic growth of the non-coplanar subsidiary cracks (in model B), which occasionally gives rise to coalescence among them, and the propagation is thus transferred to one of the non-coplanar subsidiary cracks (in model C).

In model A, dynamic rupture growth occurs only on the plane $Y=0$ in the form of coalescence with adjacent coplanar subsidiary cracks (see Fig. 4a). As the main crack grows, we can see dynamically perturbed cracks around it. Positively interacted cracks tend to appear in the region ahead of the tips of the main crack because of stress enhancement. On the other hand, negatively interacted cracks are seen around the trace of the main crack, where the main crack forms the stress shadow. The above dynamic behaviour is consistent with the inference from the static analysis of two interactive cracks in the Introduction. Propagation of the non-coplanar subsidiary cracks is not excited in this model: the stresses at the tips of the non-coplanar subsidiary cracks do not exceed the critical threshold even in the zone of increased stress formed by the main crack.

We now show the spatio-temporal crack growth path for model S, in which only the array of the coplanar pre-existing cracks at $Y=0$ is picked up out of the cracked zone model, and a slightly large crack length of 9 is assumed only for the crack at $X=0$ to initiate the dynamic growth there (see Fig. 3b). Using this as a reference model, we can investigate

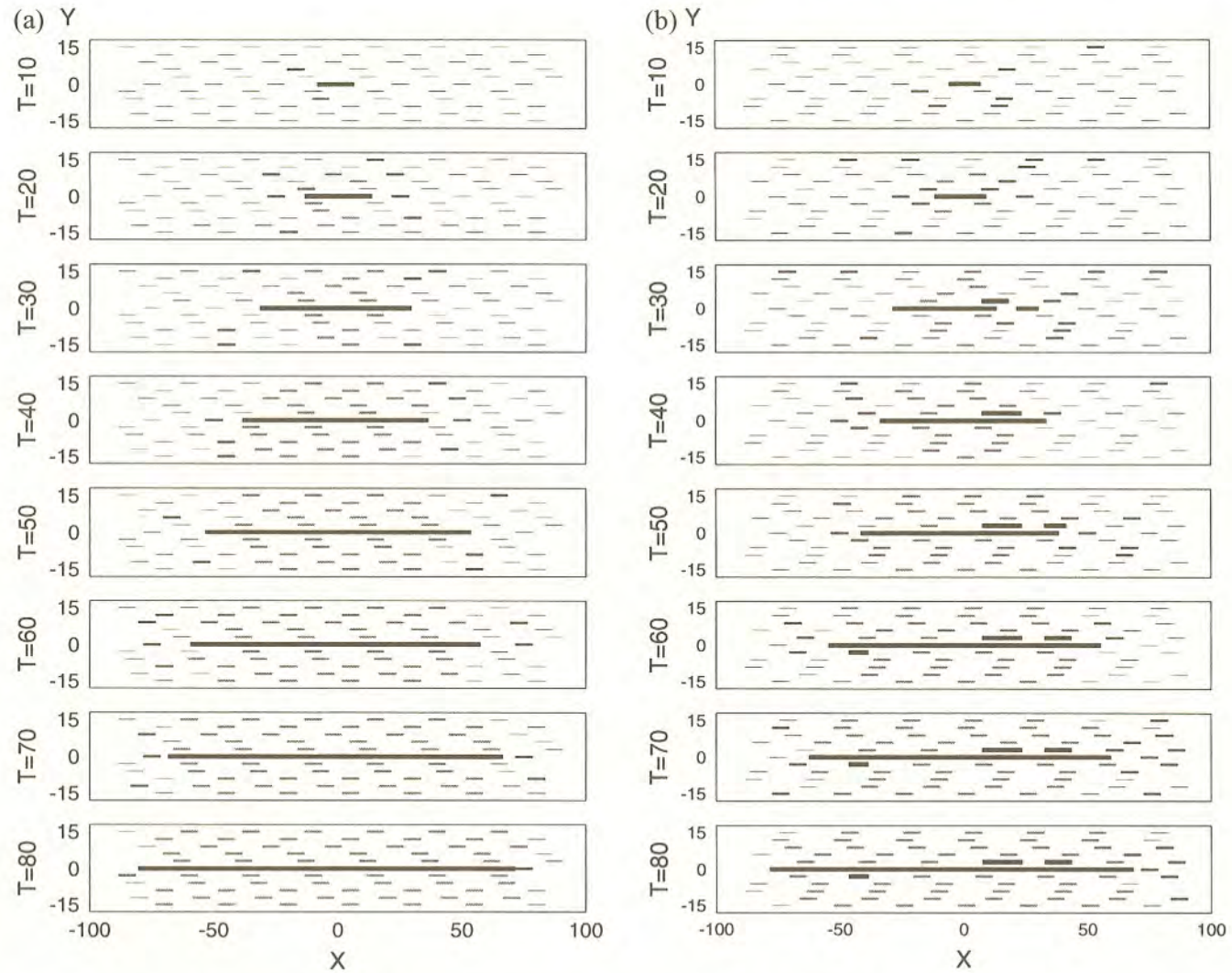

Figure 4. Snapshots of rupture propagation in the cracked zone models. At $T=0$, all the pre-existing cracks are assumed to be the same length. The thickest solid line indicates propagation-experienced cracks. Solid and grey lines with the same thickness represent the positively and negatively interacted cracks, respectively. The thinnest solid lines denote non-interacted cracks. (a) Snapshot of model A. $M_{\text{main}}=2.03$, $M_{\text{sub}}=2.14$. (b) Snapshot of model B. $M_{\text{main}}=2.27$, $M_{\text{sub}}=2.12$. (c) Snapshot of model C. $M_{\text{main}}=2.31$, $M_{\text{sub}}=2.27$.

the effect of non-coplanar crack interactions. In model S, the rupture velocity soon approaches the shear-wave velocity before the first coalescence with the adjacent two coplanar cracks at $T=21$; note that the first coalescence occurs with the right and left cracks at the same time because the rupture propagates bilaterally in a purely symmetric way without the effect of non-coplanar interactions (Fig. 5a). After the first crack tip coalescence, the rupture front passes through the pre-existing cracks at the shear-wave velocity and resumes the propagation at $T=27$ at a velocity slightly lower than the shear-wave velocity. The rupture velocity is, however, soon accelerated and again approaches the shear-wave velocity. While the main crack repeats dynamic coalescence at $T=40$, 70, and so on, the growth rate is not further accelerated, even though only coplanar interactions affect it: it has already reached the maximum allowable rupture velocity of an anti-plane crack (Kostrov 1966).

In contrast with model S, an initiated rupture in model A grows relatively slowly at the stage of the dynamic nucleation (see Fig. 5b). This suggests that the dynamic growth is decelerated by the non-coplanar crack interactions. In other words, it is interpreted that not enough strain energy can be supplied for the growth of the main crack; the stress field around the main crack before the rupture growth is already quite low, because of non-coplanar interactions among the pre-existing cracks (see Fig. 3a). The growth rate of the left crack tip at the inception of rupture is about 0.5β for $0<T<25$ before the first coalescence. The crack growth, however, accelerates with its growth. The growth rate of the left tip becomes 0.9β for $25<T<40$ between the first and the second coalescence. After several times of coalescence, the growth rate reaches the shear-wave velocity. This occurs because the growth of a largely grown crack is barely decelerated by the stress shadows of smaller non-coplanar cracks.

In model B, the main crack excites dynamic growth of non-coplanar subsidiary cracks that have their centres at $(X, Y)=(12, 3)$, $(37, 3)$ and $(-42, -3)$. Although these subsidiary cracks begin dynamic growth, their growth is soon

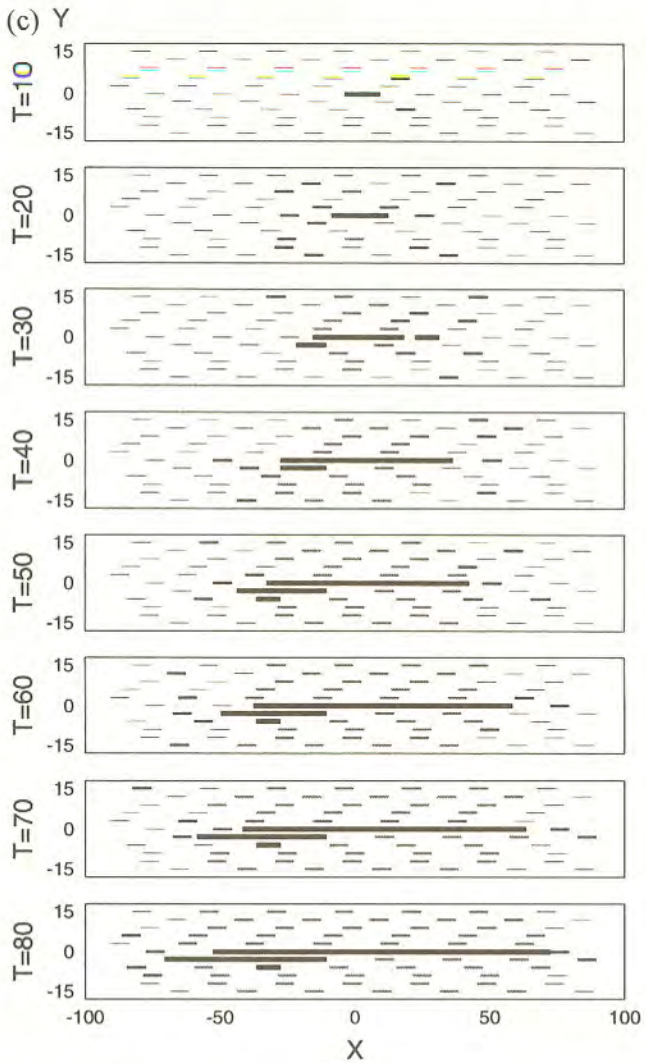

Figure 4. (*Continued.*)

arrested (see Fig. 4b); the subsidiary crack at (12, 3) begins to propagate unilaterally at $T=22$ in the $+X$-direction. The growth of the right tip of the main crack is decelerated when it comes into the stress shadow of this subsidiary crack. The main crack, however, continues to grow in spite of this transient deceleration, and then the dynamic coalescence occurs with the growing subsidiary coplanar crack on the right at $T=40$. The growing non-coplanar subsidiary crack becomes completely covered with the stress shadow of the main crack at this instant and stops its propagation. The main crack continues to propagate and again excites the growth of the non-coplanar subsidiary cracks at $(X, Y)=(37, 3)$ and $(-42, -3)$. However, the growth of these subsidiary cracks is also soon arrested because the stress shadow of the main crack is relatively large at this time.

In model C, the growth of one of the tips of the main crack is considerably decelerated and the propagation is discontinuously transferred to one of the non-coplanar subsidiary cracks on the plane $Y=-3$ (see Fig. 4c). First, the dynamic growth of the non-coplanar subsidiary crack at $(-15, -3)$ is excited by the stress increase ahead of the left tip of the main crack. Left tips of the main crack and this subsidiary crack propagate

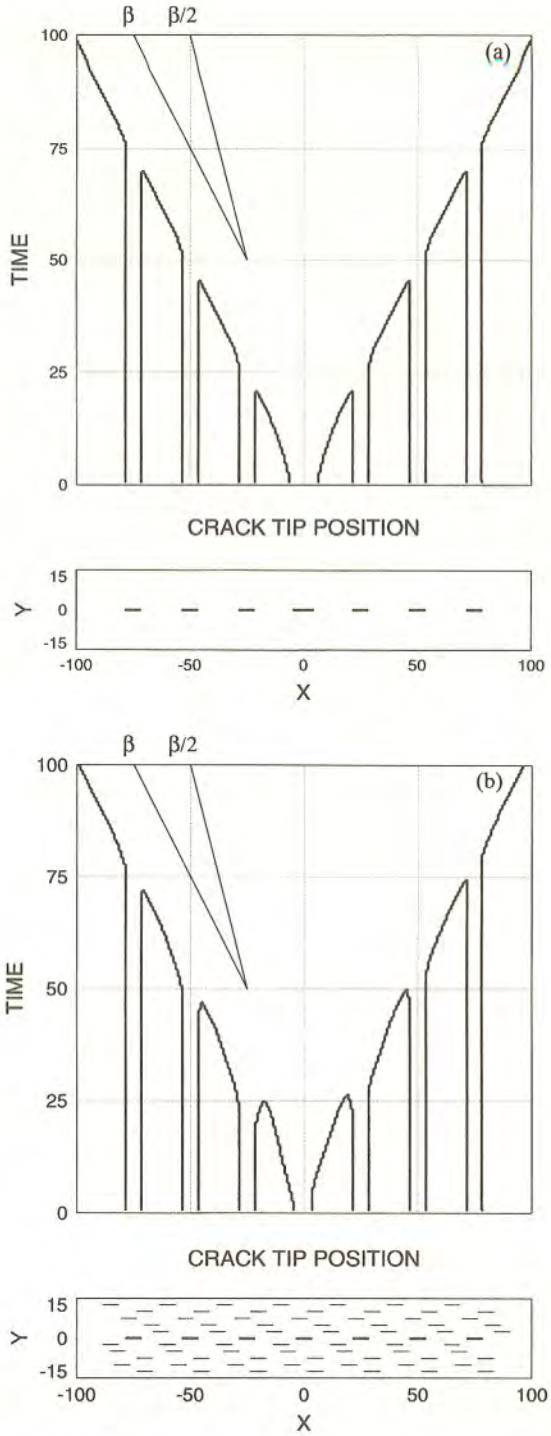

Figure 5. (a) Spatio-temporal plot of the rupture propagation paths of model S. β represents the shear-wave velocity, and $M_{\text{main}}=2.21$. (b) Spatio-temporal plot of the rupture propagation paths of model A. Note that only the coplanar cracks on the plane $Y=0$ have propagated. $M_{\text{main}}=2.03$, $M_{\text{sub}}=2.14$.

together for a while in the x-direction. In addition, another non-coplanar subsidiary crack on the plane $Y=-6$ begins dynamic growth due to the stress concentration in front of the growing subsidiary crack on the plane $Y=-3$. After a short time, coalescence of the subsidiary cracks on the plane $Y=-3$ occurs earlier than on the plane $Y=-6$. A relatively large

subsidiary crack appears due to this coalescence, and the left tip of the main crack is covered with the stress shadow of this coalesced subsidiary crack. Thus the growth of the main crack in the x-direction is highly decelerated. At the same time, the growth of the subsidiary crack on $Y=-6$ is completely arrested in the same way, and therefore the rupture growth in the x-direction is transferred from the plane $Y=0$ to $Y=-3$.

Large-scale echelon fault segments are sometimes observed after the occurrence of a larger shallow earthquake; for example, three large echelon fault segments, Johnson Valley, Homestead and Camp Rock/Emerson Faults, were observed at the time of the 1992 Landers, California, earthquake (Johnson, Fleming & Cruikshank 1994; see Fig. 6). Our results for model C seem to explain the observed echelon pattern of this fault trace if observed large-scale surface fault breaks reflect the rupture process. In fact, seismic studies have shown that some of these large surface features persist throughout the seismic zone (e.g. Moore & Byerlee 1991). In the 1995 Kobe (Hyogo-ken Nanbu) earthquake, although the main rupture did not appear entirely at the ground surface, the distribution of the hypocentres of the aftershocks suggests the existence of fault steps (Hirata *et al.* 1996). In this earthquake, inversion analysis of geodesic data additionally shows the possibility of other subsidiary ruptures on the active faults that are non-coplanar with the main one (Yoshida *et al.* 1996). It is likely that the crack interactions play a certain role in forming these geometric features of the ruputure.

Harris *et al.* (1991) and Harris & Day (1993) numerically investigated the effect of fault steps on dynamic rupture in terms of the dynamic interaction of two non-coplanar shear cracks. However, they pre-supposed the stepped geometry of the two faults and the fixed fault length in their calculations, and they did not study the effect of interactions on the spontaneous growth process of the faults. By contrast, our numerical analysis shows the possibility of forming the fault step due to the effect of interactions among dynamically growing cracks without the assumption of a pre-existing stepped structure: dynamic rupture could form the fault step with self-excited crack interactions during crack propagation.

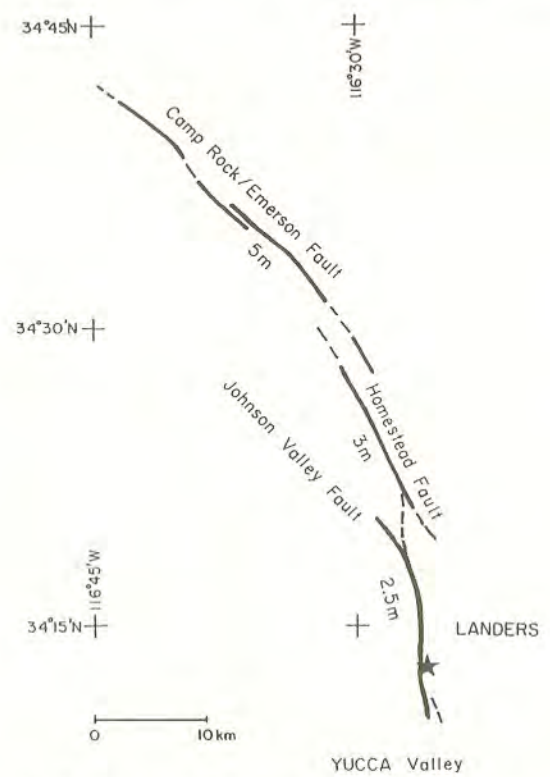

Figure 6. The fault trace of the 1992 Landers, California, earthquake (after Johnson *et al.* 1994).

VELOCITY WAVE RADIATED BY DYNAMIC NUCLEATION IN THE CRACKED ZONE

In the preceding section, we showed the dynamic rupture processes nucleated in model S, which only has a coplanar crack array, and in the cracked zone models A, B and C. In this section we present the waveforms due to these ruptures and consider how crack interactions are reflected in their features. The velocity seismograms due to the dynamic nucleation of ruptures in the cracked zones are plotted as solid curves in Fig. 7. The recorded point is assumed to be at $(X, Y)=(20, 100)$, outside the cracked zone. We use a low-pass filter for the velocity seismogram after taking the time derivative of the displacement to remove high-frequency numerical errors. We also plot in Fig. 7 the seismogram with a broken curve for model S for the sake of comparison. We find a characteristic feature in the seismograms radiated from the cracked zone models: the onsets of the velocity waves are generally gradual, and the velocities undergo a sudden increase after a short time. This seems to account for the two distinct phases, P_1 and P_2, observed in a large shallow earthquake. On the other hand, the velocity wave emitted from model S has a much steeper onset, which does not have the feature of the P_1 phase. The contrast between the velocity seismograms for the coplanar crack array model and the cracked zone model enables us to attribute the gradual onset phase radiated from the cracked zone model to the effect of the non-coplanar interactions in a cracked zone.

We now consider in detail the radiation mechanism of the velocity waves observed in Fig. 7 in terms of crack interactions; models S and A are employed in the consideration. As stated

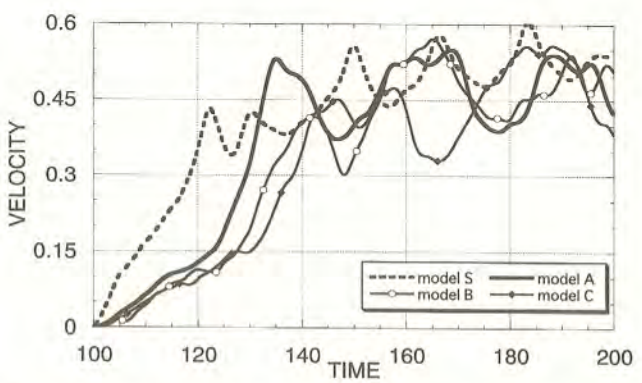

Figure 7. Non-dimensional velocity seismograms recorded outside the cracked zone at $X=20$ and $Y=100$. The solid curves and the broken curve stand for the velocity waveforms radiated by the rupture in the cracked zone models and model S, respectively. These are obtained by low-pass filtering the original data at the non-dimensional frequency 0.025.

before, the crack interactions exert two conflicting effects: one tends to accelerate the crack growth, and the other tends to decelerate it. The accelerating and decelerating effects are generally ascribable to the coplanar and non-coplanar interactions, repectively. Note that only the coplanar crack interactions arise in model S. Accordingly, the dynamic growth is well accelerated from the first and the growth rate soon approaches the shear-wave velocity before the first coalescence at $T = 20$ (see Fig. 5a). The steep build-up at the onset of the waveform ($T = 100$–122) shown by the broken curve in Fig. 7 is radiated by this accelerated nucleation of dynamic rupture. After the accelerating stage, the growth rate remains close to the shear-wave velocity and the propagating crack repeats the coalescence with neighbouring coplanar cracks, as shown in Fig. 5(a). This repeated coalescence gives rise to the peaks in the velocity seismogram at $T = 122, 130, 150, \ldots$, which are ascertained from the ray theoretical calculation of the arrival time of the elastic wave radiated by the rupture; it is theoretically known that the dynamic crack coalescence can be a source of high-frequency elastic wave radiation (Madariaga 1983).

We next consider the elastic wave radiation from the rupture growth in model A. Compared with the rupture in model S, the crack growth in model A is less accelerated at its dynamic nucleation (see Fig. 5b). This is due to the relative predominance of the non-coplanar crack interactions at the initial stage of rupture, and this relatively slow rupture leads to the gradual onset of the velocity seismogram ($T = 100$–123) plotted as the thick solid curve in Fig. 7. The first nucleated crack, however, continues to grow even in predominantly non-coplanar interaction. After a short time, the transition occurs from the state of non-coplanar interaction predominance to that of coplanar interaction predominance. This is due to the approach of the growing crack to the neighbouring cracks on both sides and their coalescence at $T = 25$–27; note that coplanar interaction begins to prevail when two cracks come close to each other, and the sudden appearance of the large coalesced crack makes the non-coplanar interaction less dominant. As a result of this transition, the crack growth rate becomes highly accelerated. The abrupt increase in the velocity seismogram at $T \cong 123$ is caused by the change in the crack growth rate during this accelerating stage. In addition to crack coalescence, the abrupt change in crack propagation velocity is known to be another source of high-frequency elastic wave radiation (Madariaga 1977; Yamashita 1983). The gradual onset and abrupt change at $T \cong 123$ in the velocity seismogram are therefore interpreted to be radiated in the process of the transition from predominantly non-coplanar to coplanar interaction. After the first coalescence, the propagating crack coalesces with the neighbouring cracks again and again, maintaining a high rupture velocity. Later abrupt changes in the velocity seismogram of model A are also associated with the crack coalescence. For example, the abrupt increase at $T = 147$ is due to the coalescence of the propagating crack with the cracks whose centres are at $X = -50$ and $X = 50$ on the plane $Y = 0$ (see Fig. 5b). The decrease beginning at $T = 134$ in the solid curve is caused by the temporary deceleration of crack growth after the first coalescence: this deceleration occurs because the effects of coplanar crack interactions become temporarily less dominant after the completion of crack coalescence.

In our numerical analysis, the crack distribution before the dynamic growth is presumed so that the non-coplanar crack interactions are dominant. From the seismological viewpoint, it seems reasonable to assume such a distribution of cracks before the occurrence of a large shallow earthquake. Strain energy will be much accumulated before the occurrence of a large shallow earthquake in its epicentral region. It has, however, been pointed out that a period of seismic quiescence exists in such a region before the occurrence of the earthquake (Mogi 1969, 1979; Ohtake 1976; Ohtake, Matsumoto & Latham 1977). This premonitory phenomenon is termed a seismic gap of the second kind (Mogi 1979). This suggests that the occurrence of earthquakes is totally suppressed in the future epicentral area in this time. We consider that the seismicity that precedes the emergence of quiescence is associated with growth of the pre-existing cracks preparing for the main shock. With their growth, the stress shadow area of each crack tends to overlap the others, and the non-coplanar interactions will become relatively dominant. Dynamic crack growth therefore becomes suppressed and the seismic quiescence will emerge. In fact, Yamashita & Knopoff (1992) showed in their simulations of seismicity in a cracked zone that the dominance of non-coplanar crack interactions is a key ingredient for the seismic quiescence before the occurrence of a large event; as long as coplanar interactions are dominant in a fault zone, it is expected that seismic activity becomes more notable nearer the main shock, and the seismic quiescence is not observed. We can therefore infer that non-coplanar crack interaction becomes dominant immediately before the ocurrence of a large shallow earthquake as long as the cracked zone model is appropriate.

Umeda (1990) showed that the P_1 phase is not observed for aftershocks even if they are large enough (see Fig. 8). This observation is consistent with our interpretation for the generation mechanism of the P_1 phase. We consider that many pre-existing cracks grow quasi-statically and/or dynamically, into large ones in the fault zone of the eventual large earthquake before its occurence. After the pre-existing cracks have grown large, the non-coplanar interaction predominance is attained. However, once a main shock occurs, a predominantly large

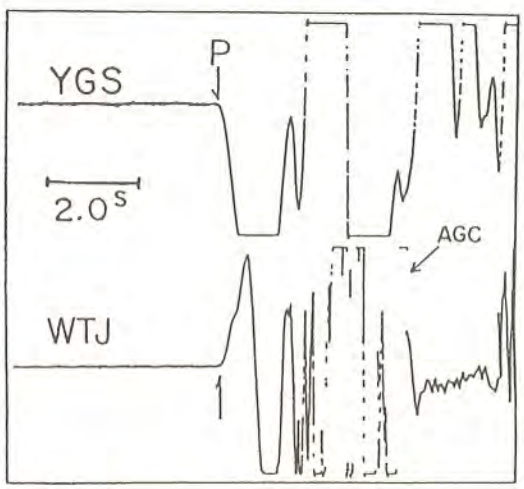

Figure 8. Vertical seismograms emitted from an aftershock ($M = 6.2$) of the 1984 Western Nagano earthquake (after Umeda 1990). These were recorded at the same observation stations as for the main shock in Fig. 1(a). Note that the magnitude of this event is comparable to that of the main shock, whose seismograms are shown in Fig. 1(a).

fault appears and the coplanar interactions will be predominant where the aftershock occurs. This does not cause the slow onset P_1 phase in seismograms of aftershocks according to our modelling results; in our model, the pre-existing cracks need to have grown to a large enough size to cause non-coplanar interactions before the occurrence of rupture for the appearance of the preliminary rupture phase.

GENERATION MECHANISM OF THE EARTHQUAKE BRIGHT SPOT

The generation of high-frequency strong motion in earthquakes is a matter of concern in engineering seismology. Here, we take a topic of an earthquake bright spot related to the radiation of strong high-frequency seismic waves and argue its generation mechanism in terms of the pre-existing cracks in a fault zone.

Umeda (1981, 1990, 1992) found from field observation of ejected boulders and surface cracks near faults that the source area of strong high-frequency seismic wave radiation is commonly localized for large shallow earthquakes. It is characteristic that the dimension of this area is far smaller than the total rupture area and its location tends to be near the epicentre. Umeda (1990) termed this small region the 'earthquake bright spot'. The feature of the bright spot is also supported by inversion analyses using strong-motion waveforms. For the 1995 Kobe earthquake, the region of the strong wave radiation is determined to be close to the hypocentre (Ide, Takeo & Yoshida 1996; Yoshida *et al.* 1996). The 1994 Northridge earthquake provides another example (Dreger 1994). It is noteworthy that the bright spot in the 1989 Loma Prieta earthquake observed by Umeda (1992) was located precisely above the source of the strongest high-frequency radiation that was determined by Zeng, Aki & Teng (1993) using strong-motion data.

Our fault zone model enables us to give an interpretation of the feature of the earthquake bright spot. A crack tip velocity shows a sudden increase soon after its nucleation because of the sudden transition from non-coplanar to coplanar interaction predominance due to the approach of the first nucleated crack to the adjacent cracks and their subsequent coalescence. This suggests that high-frequency acceleration can be efficiently radiated in the early stages of crack propagation since the radiated energy is generally larger for a larger change in crack tip velocity (Madariaga 1977; Yamashita 1983). The acceleration seismogram corresponding to the velocity waveform of model A is plotted in Fig. 9; the highest acceleration is certainly radiated by the coalescence of the first nucleated crack with the neighbouring cracks on both sides at $T = 25$–27. We consider that this is a reason why an earthquake bright spot tends to be formed relatively close to the epicentre. This model for the earthquake bright spot marks an improvement on the model by Yamashita & Umeda (1994), in which the bright spot does not necessarily have to be formed close to the hypocentre: according to their model, an earthquake bright spot can be formed in any localized area where nucleation and propagation arresting of several cracks occur.

DISCUSSION AND CONCLUSIONS

We investigated in this paper the dynamic nucleation mechanism of large shallow earthquake faulting. On the basis of seismological observations of fault zones, we constructed a fault zone model as an interactive system: densely distributed pre-existing cracks were assumed and multiple interactions among them were rigorously treated. We carried out theoretical calculations to examine the defects of crack interactions on the initial stage of the dynamic crack growth.

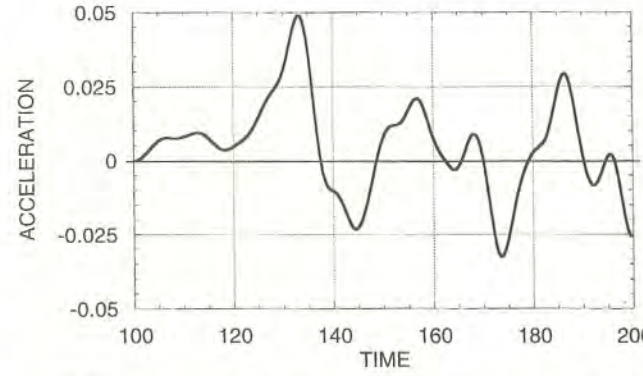

Figure 9. Non-dimensional accelerogram corresponding to the velocity seismogram of model A represented by the thick solid line in Fig. 7. Low-pass filtering at the non-dimensional frequency 0.025 has been carried out.

Our result showed that the two distinct phases, P_1 and P_2, commonly observed in the seismograms of large shallow earthquakes can be interpreted as a manifestation of the transition process from non-coplanar to coplanar interaction predominance in a fault zone; the growth rate of the propagating crack changes from low to high due to the transition, and this process radiates the above two phases. It is essential for the radiation of the preliminary rupture phase, P_1, that the non-coplanar interactions are predominant among the pre-existing cracks. It was also shown that the fault step geometry can be formed by the self-excited crack interactions during crack propagation: a propagating crack excites growth of the other non-coplanar cracks, which occasionally arrests the propagating crack and discontinuous transfer of the propagation occurs.

We proposed a generation mechanism of the earthquake bright spot. What is essential for the appearance of the bright spot is the relative predominance of the non-coplanar crack interactions that brings about the slow growth rate of the first nucleated crack. The nucleated crack will otherwise soon be accelerated and therefore coalescence will rarely result in a large change in the crack growth rate, which is the source of a high-frequency strong wave.

The concept of asperity has been introduced to account for the heterogeneity of wave radiation in earthquake faulting (Lay & Kanamori 1981). This concept has been employed by many researchers (e.g. Ruff & Kanamori 1983). However, the physical nature of such a concept remains obscure. Our analysis shows that dynamic crack interactions at the nucleation stage of a large earthquake can be one of the physical realities of local strong wave radiation.

Seismological observation shows the positive scaling between the duration of the dynamic nucleation phase and the earthquake magnitude (Umeda 1992; Ellsworth & Beroza 1995). The arresting mechanism of fault propagation is absolutely necessary to understand the above observation. However, our main concern is with the dynamic nucleation of earthquake rupture, and so we did not consider the arresting mechanism.

Further study is required to explain the scaling relation quantitatively.

We have a highly simplified assumption in the theoretical calculation, which is that all the cracks are parallel and that each crack propagates only on its own plane. Accordingly, connection with a non-coplanar crack and crack bifurcation are not supposed to occur, although such phenomena are sometimes observed geologically in a fault zone. The effects of such phenomena will also have to be examined in future studies. We consider that their effects should influence the formation of a fault step. Crack tip velocity will also be changed by their effects. For example, Umeda (1990) found three fault branches at the bright spot of the 1990 Philippine earthquake. A more complicated crack configuration (e.g. crack curvature and crack bifurcation) will be necessary for a more realistic application of our model.

ACKNOWLEDGMENTS

This research was supported in part by a grant from the Ministry of Education, Science and Culture of Japan (project 06680423). Computation time was provided by the Supercomputer Laboratory, Institute for Chemical Research, Kyoto University.

REFERENCES

Abe, K., 1990. Seismological aspects of the Luzon, Philippine earthquake of July 16, 1990, *Bull. Earthq. Res. Inst.*, **65,** 851–873 (in Japanese, with English abstract).

Abercrombie, R. & Mori, J., 1994. Local observations of the onset of a large earthquake: 28 June 1992 Landers, California, *Bull. seism. Soc. Am.*, **84,** 725–734.

Cochard, A. & Madariaga, R., 1994. Dynamic faulting under rate-dependent friction, *Pageoph,* **142,** 419–445.

Das, S. & Aki, K., 1977. Fault plane with barriers: a versatile earthquake model, *J. geophys. Res.*, **82,** 5658–5670.

Dreger, D.S., 1994. Empirical Green's function study of the January 17, 1994 Northridge, California, earthquake, *Geophys. Res. Lett.*, **21,** 2633–2636.

Ellsworth, W.L. & Beroza, G.C., 1995. Seismic evidence for an earthquake nucleation phase, *Science,* **268,** 851–855.

Harris, R.A. & Day, S.M., 1993. Dynamics of fault interaction: parallel strike-slip faults, *J. geophys. Res.*, **98,** 4461–4472.

Harris, R.A., Archuleta, R.J. & Day, S.M., 1991. Fault steps and the dynamic rupture process: 2-d numerical simulations of a spontaneously propagating shear fracture, *Geophys. Res. Lett.*, **18,** 893–896.

Hirata, N., *et al.*, 1996. Urgent Joint Observation of Aftershocks of the 1995 Hyogo-ken Nanbu Earthquake, *J. Phys. Earth,* **44,** in press.

Ide, S., Takeo, M. & Yoshida, Y., 1996. Source process of the 1995 Kobe earthquake: Determination of spatio-temporal slip distribution by Bayesian modeling, *Bull. seism. Soc. Am.*, **86,** 547–566.

Johnson, A.M., Fleming, R.W. & Cruikshank, K.M., 1994. Shear zones formed along long straight traces of fault zones during the 28 June 1992 Landers, California, earthquake, *Bull. seism. Soc. Am.*, **84,** 499–510.

Kostrov, B.V., 1966. Unsteady propagation of longitudinal shear cracks, *J. appl. Math. Mech.*, **30,** 1241–1248.

Lay, T. & Kanamori, H., 1981. An asperity model of great earthquake sequences, in *Earthquake prediction,* Vol. 4, pp. 579–592, eds Sinpson, D.W. & Richards, P.G., American Geophysical Union, Maurice Ewing Series.

Leary, P.C., Li, Y.G. & Aki, K., 1987. Observation and modelling of fault-zone fracture seismic anisotropy, I. P, SV and SH travel times, *Geophys. J. R. astr. Soc.*, **91,** 461–484.

Madariaga, R., 1977. High frequency radiation from crack (stress drop) models of earthquake faulting, *Geophys. J. R. astr. Soc.*, **51,** 625–651.

Mogi, K., 1969. Some features of recent seismic activity in and near Japan (2): Activity before and after great earthquakes, *Bull. Earth. Res. Inst.*, **47,** 395–417.

Mogi, K., 1979. Two kinds of seismic gaps, *Pageoph,* **117,** 1172–1186.

Moore, D.E. & Byerlee, J.D., 1991. Comparison of the San Andreas fault, California, and laboratory fault zones, *Geol. Soc. Am. Bull.*, **103,** 762–774.

Ohtake, M., 1976. Search for precursors of the 1974 Izu-Hanto-oki earthquake, Japan, *Pageoph,* **114,** 1083–1093.

Ohtake, M., Matsumoto, T. & Latham, G.V., 1977. Seismic gap near Oaxaca, Southern Mexico, as a possible precursor to a large earthquake, *Pageoph,* **115,** 375–385.

Rice, J.R., 1992. Fault stress state, pore pressure distributions, and the weakness of the San Andreas Fault, in *Fracture Mechanics and Transport Properties of Rocks,* pp. 475–503, eds Evans, E.B. & Wong, T.F., Academic, London.

Ruff, L. & Kanamori, H., 1983. The rupture process and asperity distribution of three great earthquakes from long-period diffracted P waves, *Phys. Earth planet. Inter.*, **31,** 202–230.

Shibazaki, B. & Matsu'ura, M., 1992. Spontaneous process for nucleation, dynamic rupture propagation, and stop of earthquake rupture, *Geophys. Res. Lett.*, **19,** 1189–1192.

Scholz, C.H., 1990. Earthquakes as chaos, *Nature,* **348,** 197–198.

Tchalenko, J.S., 1970. Similarities between shear zones of different magnitudes, *Bull. geol. Soc. Am.*, **81,** 1620–1640.

Tchalenko, J.S. & Berberian, M., 1975. Dasht-e Bayez fault, Iran: Earthquake and earlier related structures in bed rock, *Geol. Soc. Am. Bull.*, **86,** 703–709.

Umeda, Y., 1981. An earthquake source model with a ripple generating core, *J. Phys. Earth,* **29,** 341–370.

Umeda, Y., 1990. High-amplitude seismic waves radiated from the bright spot of an earthquake, *Tectonophysics,* **175,** 81–92.

Umeda, Y., 1992. The bright spot of an earthquake, *Tectonophysics,* **211,** 13–22.

Umeda, Y., Kuroiso, A., Ito, K. & Muramatsu, I., 1987. High accelerations produced by the western Nagano prefecture, Japan, earthquake of 1984, *Tectonophysics,* **141,** 335–343.

Umeda, Y., Yamashita, T., Tada, T. & Kame, N., 1996. Possible mechanism of dynamic nucleation and arresting of shallow earthquake faulting, *Tectonophysics,* **261,** 179–192.

Yamashita, T., 1983. High-frequency acceleration radiated by unsteadily propagating cracks and its near-source geometrical attenuation, *J. Phys. Earth,* **31,** 1–32.

Yamashita, T., 1995. Simulation of seismicity due to ruptures on non-coplanar interactive faults, *J. geophys. Res.*, **100,** 8339–8350.

Yamashita, T. & Knopoff, L., 1992. Model for intermediate-term precursory clustering of earthquakes, *J. geophys. Res.*, **97,** 19 873–19 879.

Yamashita, T. & Fukuyama, E., 1996. Apparent critical slip displacement caused by the existence of a fault zone, *Geophys. J. Int.*, **125,** 459–472.

Yamashita, T. & Umeda, Y., 1994. Earthquake rupture complexity due to dynamic nucleation and interaction of subsidiary faults, *Pageoph,* **143,** 89–116.

Yoshida, S., Koketsu, K., Shibazaki, B., Sagiya, T., Kato, T. & Yoshida, Y., 1996. Joint inversion of near- and far-field waveforms and geodectic data for the rupture process of the 1995 Kobe earthquake, *J. Phys. Earth,* **44,** in press.

Zeng, Y., Aki, K. & Teng, T., 1993. Mapping of the high-frequency source radiation for the Loma Prieta earthquake, California, *J. geophys. Res.*, **98,** 11 981–11 993.

APENDIX A: MATHEMATICAL ANALYSIS OF THE DYNAMIC GROWTH OF INTERACTIVE CRACKS

We briefly review the method of analysis used by Yamashita & Fukuyama (1996), which is mostly based on the analysis of Cochard & Madariaga (1994).

Consider an infinite homogeneous elastic medium, which is in static equilibrium for $t<0$. All the cracks are assumed to appear suddenly at $t=0$, and to be aligned parallel each other. The dynamic displacement u is related to the relative slip on each crack by the convolution (Cochard & Madariaga 1994)

$$u(x, y, t)=\sum_{p=1}^{N}\int_{\Gamma_p}\int_0^t \Delta u_p(\xi, \tau)F(x, y-y_p, \xi, t-\tau)\,d\xi d\tau, \quad \text{(A1)}$$

where N is the number of cracks, $\Delta u_p = u(x, y_p+0, t) - u(x, y_p-0, t)$ is the relative slip across the pth crack Γ_p ($p=1, \ldots, N$), y_p is the y coordinate of the pth crack, and F is the yz component of the stress tensor associated with the 2-D Green's function

$$G(x, y, \xi, t)=\frac{1}{2\pi\mu}\frac{H(t-r/\beta)}{\sqrt{t^2-r^2/\beta^2}}. \quad \text{(A2)}$$

$H(\cdot)$ is a unit step function, β is the shear-wave velocity, μ is the rigidity and $r=\sqrt{(x-\xi)^2+y^2}$. The stress component σ_{yz} is assumed to be given on each crack Γ_p ($p=1, \ldots, N$) in the form

$$\sigma_{yz}(x, y_j, t)=-\sigma_0, \quad \text{(A3)}$$

as the boundary condition. We obtain the following integral equation on each crack by transforming eq. (A1) (Cochard & Madariaga 1944):

$$\sigma_{yz}(x, y, t)=-\frac{\mu}{2\pi}\sum_{p=1}^{N}\left[\frac{1}{\beta^2}\int_{\Gamma_p}d\xi\int_0^{\tau_m}\frac{\partial}{\partial\tau}\Delta\dot{u}_p(\xi, \tau)\times\frac{d\tau}{\sqrt{(t-\tau)^2-r^2/\beta^2}}+\int_{\Gamma_p}\frac{x-\xi}{(x-\xi)^2+(y-y_p)^2}d\xi\times\int_0^{\tau_m}\frac{\partial}{\partial\xi}\Delta\dot{u}_p(\xi, \tau)\frac{t-\tau}{\sqrt{(t-\tau)^2-r^2/\beta^2}}d\tau\right], \quad \text{(A4)}$$

where $r_j=\sqrt{(x-\xi)^2+(y-y_j)^2}$, and the dot denotes the partial differentiation with respect to time τ. The physical quantities are normalized by an arbitrary unit of length L and the rigidity of the medium μ in the following calculations. The non-dimensional coordinates are therefore given by $X=x/L$, $Y=y/L$, and $T=\beta t/L$; the stress and displacement are given by $S=\sigma_{yz}/\mu$ and $U=u/L$. Using the technique developed by Cochard & Madariaga (1994), we then obtain the discretized non-dimensional integral equation,

$$S_{i,k}^{j}=-\frac{1}{2\pi}\sum_{p=1}^{N}\sum_{n=0}^{k}\sum_{l}V_{l,n}^{m_p}\Pi_{i-l,k-n}^{j-m_p}, \quad \text{(A5)}$$

on the crack surfaces where the summation with respect to l is carried out over the slipped area. Here, $V_{l,n}^{m_p}$ is the non-dimensional slip velocity on the pth crack defined on the rectangular element $X_l \le X \le X_{l+1}=X_l+\Delta X$ and $T_n \le T \le T_{n+1}=T_n+\Delta T$, and $S_{i,k}^{j}$ is the non-dimensional stress at $X=(i+1/2)\Delta X, Y=j\Delta X$ and $T=(k+1/2)\Delta X$. We set $2\Delta T=\Delta X=1$ in the calculations. When a rectangular element of the slip velocity is completely contained in the wave cone, the corresponding expression for $\Pi_{i,k}^{j}$ is given by

$$\Pi_{i,k}^{j}=R_{i,k+1}^{j}-R_{i,k}^{j}-R_{i-1,k+1}^{j}+R_{i-1,k}^{j}, \quad \text{(A6)}$$

where

$$R_{i,k}^{j}=\frac{i+1/2}{(i+1/2)^2+j^2}\sqrt{k^2/4-(i+1/2)^2-j^2}+\sin^{-1}\frac{i+1/2}{\sqrt{k^2/4-j^2}}. \quad \text{(A7)}$$

When $S_{i,k}^{j}$ is given on each crack surface as the boundary condition, the slip velocity is obtained from eq. (A5) at any time step k in the form

$$V_{i,k}^{j_p}=-\frac{2\pi}{\Pi_{0,0}^{0}}S_{i,k}^{j_p}-\frac{1}{\Pi_{0,0}^{0}}\sum_{q=1}^{N}\sum_{n=0}^{k-1}\sum_{l}V_{l,n}^{m_q}\Pi_{i-l,k-n}^{j_p-m_q}, \quad \text{(A8)}$$

where $\Pi_{0,0}^{0}=\pi$. When it comes to treating non-coplanar cracks, short-wavelength oscillation in slip velocity becomes evident and grows to the point of invalidating the solution due to multiply reflected waves among them. Yamashita & Fukuyama (1996) eliminated this phenomenon, introducing a damping term into eq. (A8):

$$V_{i,k}^{j_p}=-\frac{2\pi}{\Pi_{0,0}^{0}}S_{i,k}^{j_p}-\frac{1}{\Pi_{0,0}^{0}}\sum_{q=1}^{N}\sum_{n=0}^{k-1}\sum_{l}V_{l,n}^{m_q}\Pi_{i-l,k-n}^{j_p-m_q}+\alpha(V_{i-1,k}^{j_p}+V_{i+1,k}^{j_p}-2V_{i,k}^{j_p}), \quad \text{(A9)}$$

where α is the damping coefficient. We set α to be 0.5, the same value used in Yamashita & Fukuyama (1996). It was shown in previous studies (Cochard & Madariaga 1994; Yamashita & Fukuyama 1996) that the accuracy of this method is quite satisfactory.

When pre-existing cracks are treated, we first determine the static pre-slips on them (see Appendix B). After setting up these pre-slips at time step $k=0$, we begin the calculation of the slip velocity due to the dynamic process. We slightly change eq. (A3) to take the static pre-slip $D_{i,\text{static}}^{j}$ into account, giving

$$V_{i,k}^{j_p}=-\frac{2\pi}{\Pi_{0,0}^{0}}S_{i,k}^{j_p}-\frac{1}{\Pi_{0,0}^{0}}\times\left(\sum_{q=1}^{N}\sum_{n=1}^{k-1}\sum_{l}V_{l,n}^{m_q}\Pi_{i-l,k-n}^{j_p-m_q}+\sum_{q=1}^{N}\sum_{l_0}D_{l_0,\text{static}}^{m_q}\Pi_{i-l_0,\infty}^{j_p-m_q}\right), \quad \text{(A10)}$$

where l_0 represents the pre-existing crack. The damping term is eliminated for simplicity. As long as no pre-existing cracks begin dynamic propagation, eq. (A10) gives zero slip velocity on them.

Once the slip velocity $V_{i,k}^{j_p}$ is obtained, the emitted displacement wave can be calculated from a discretized form of eq. (A1) as

$$H_{i,k}^{j}=\frac{\Delta X}{2\pi}\sum_{p=1}^{N}\sum_{n=1}^{k}\sum_{l}V_{l,n}^{m_p}\Lambda_{i-l,k-n}^{j-m_p}, \quad \text{(A11)}$$

where $H_{i,k}^{j}$ is the displacement at $X=X_i+\Delta X/2$, $Y=Y_j$, $T=T_k+\Delta T$. The expression for $\Lambda_{i,k}^{j}$ is given by

$$\Lambda_{i,k}^{j}=Q_{i,k+1}^{j}-Q_{i,k}^{j}-Q_{i-1,k+1}^{j}+Q_{i-1,k}^{j}, \quad \text{(A12)}$$

where

$$Q^j_{i,k} = -j \sin^{-1} \frac{(i+1/2)}{\sqrt{k^2/4 - j^2}} + \frac{jk}{2|j|} \times \tan^{-1} \frac{k}{2|j|} \frac{i+1/2}{\sqrt{k^2/4 - j^2 - (i+1/2)^2}}. \quad \text{(A13)}$$

APPENDIX B: SOLUTION FOR STATIC PRE-SLIPS

Consider that the slip velocity has non-zero components only for time steps $k = 1, \ldots, M$ on all the cracks; after the time step $k = M + 1$ relative slips on all the cracks will not change with time. The stress at the time step $k(\gg M)$ due to the non-zero velocity components is calculated by eq. (A5):

$$S^j_{i,k} = -\frac{1}{2\pi} \sum_{p=1}^{N} \sum_{n=0}^{k} \sum_{l} V^{m_p}_{l,n} \Pi^{j-m_p}_{i-l,k-n}.$$

In the limit $k = +\infty$, all the components of stress kernel $\Pi^{j-m_p}_{i-l,k-1}$, $\Pi^{j-m_p}_{i-l,k-2}, \ldots, \Pi^{j-m_p}_{i-l,k-M}$ converge on $\Pi^{j-m_p}_{i-l,\infty}$, which has the following form:

$$\Pi^j_{l,\infty} \equiv \lim_{k\to\infty} \Pi^j_{l,k} = \frac{1}{2}\left[\frac{i+1/2}{(i+1/2)^2 + j^2} - \frac{i-1/2}{(i-1/2)^2 + j^2}\right]. \quad \text{(B1)}$$

It is obvious that $\Pi^j_{l,\infty}$ is independent of time and only a function of position. The stress thus determined in the limit $k = +\infty$ is denoted as $S^j_{l,\text{static}}$ and is represented by

$$S^j_{i,\text{static}} = -\frac{1}{2\pi} \sum_{p=1}^{N} \sum_{l} \left(\sum_{n=1}^{M} V^{m_p}_{l,n} \Pi^{j-m_p}_{i-l,\infty} \right) = -\frac{1}{2\pi} \sum_{p=1}^{N} \sum_{l} D^{m_p}_{l,\text{static}} \Pi^{j-m_p}_{i-l,\infty}. \quad \text{(B2)}$$

The above equation clearly shows that $S^j_{i,\text{static}}$ depends only on the time sum of the velocity components, $D^{m_p}_{l,\text{static}} \equiv \Sigma_{n=1}^{M} V^{m_p}_{l,n}$. $D^{m_p}_{l,\text{static}}$ is termed the 'static pre-slip' (strictly speaking, the static pre-slip is the product of $D^{m_p}_{l,\text{static}}$ and ΔT). Eq. (B2) represents the fact that the static pre-slips $D^{m_p}_{l,\text{static}}$ on Γ_p $(p = 1, 2, \ldots, N)$ cause the static stress field $S^j_{i,\text{static}}$ everywhere including the crack surface.

When we apply eq. (B2) to all the elements on the pre-existing cracks, we have simultaneous integral equations. We use them for the determination of the static pre-slips on the pre-existing cracks that are in an equilibrium state with stress drop ΔS. Let all the pre-existing cracks have the same length $L\Delta X$ in the discretized form. L is the number of elements on a crack. Each element on crack Γ_p is numbered as (i_{p1}, j_p), $(i_{p2}, j_p), \ldots, (i_{pL}, j_p)$. Applying eq. (B2) to all the elements, we derive $L \times N$ equations that contain $L \times N$ unknown elements of the static pre-slip,

$$-\Delta S = -\frac{1}{2\pi} \sum_{q=1}^{N} \sum_{s=1}^{L} D^{m_q}_{l_{qs},\text{static}} V^{j_p - m_q}_{i_{pr} - l_{qs},\infty} \quad (p = 1, 2, \ldots, N)(r = 1, 2, \ldots, L). \quad \text{(B3)}$$

Eqs (B3) can be solved numerically by using the matrix inversion, and the pre-slips are determined. Once the static pre-slips on the pre-existing cracks are determined, the static stress field is calculated using eq. (B2).